actuators

MDPI

Article

Multi-Objective Parameter Optimization of Rotary Screen Coating Process for Structural Plates in Spacecraft

Yanhui Guo [1], Yanpeng Chen [2], Peibo Li [1,*], Xinfu Chi [1] and Yize Sun [1]

[1] College of Mechanical Engineering, Donghua University, Shanghai 201620, China; 1179182@mail.dhu.edu.cn (Y.G.)
[2] Shanghai Institute of Spacecraft Equipment, Shanghai 200240, China
* Correspondence: leonlee@dhu.edu.cn

Abstract: A multi-objective grasshopper optimization algorithm (MOGOA) with an adaptive curve c(t) and the enhanced Levy fight strategy (CLMOGOA) was proposed to optimize the process parameters of rotary screen coating, setting the thickness and uniformity of the adhesive layer on the structural plates in spacecraft as its optimization objectives. The adaptive curve strikes a balance between global exploration and local development and accelerates the convergence speed. The enhanced Levy strategy helps the algorithm to escape local optimizations, increases the population diversity, and possesses dual searching capabilities. After multiple runs, the average values of the CLMOGOA's reverse generation distance were 0.0288, 0.0233, and 0.1810 on the test sets, which were less than those of the MOGOA. The best Pareto-optimal front obtained by the CLMOGOA had a higher accuracy and better coverage compared to that of the MOGOA. Thus, it is indicated that the CLMOGOA managed to outperform the MOGOA on the test functions. In order to solve the optimization problem, 108 sets of process experiments were designed, and then the experimental data were used to train a Back Propagation Neural Network (BPNN), a Least Squares Support Vector Machine (LSSVM), and Random Forest (RF) to obtain the best prediction model for the process parameters. Considering the thickness and uniformity of the adhesive layer as the objectives, the improved algorithm was used to optimize the prediction model to obtain the optimal process parameters. The actual coating effect showed that the optimization algorithm improved the efficiency and qualification rate of the product.

Keywords: multi-objective optimization algorithm; optimal process parameters; rotary screen coating; prediction model; spacecraft structural plates

Citation: Guo, Y.; Chen, Y.; Li, P.; Chi, X.; Sun, Y. Multi-Objective Parameter Optimization of Rotary Screen Coating Process for Structural Plates in Spacecraft. *Actuators* **2024**, *13*, 469. https://doi.org/10.3390/act13120469

Academic Editor: Keigo Watanabe

Received: 22 October 2024
Revised: 13 November 2024
Accepted: 15 November 2024
Published: 22 November 2024

1. Introduction

In recent years, with the progress in science and technology, space exploration has become increasingly widespread [1–3], and the demand for spacecraft is also increasing. With structural plates in spacecraft being the most important structures, production efficiency has also become a concern. The coating of adhesives onto the surface of structural plates is an important step in the manufacturing process. Manual coating methods have high labor and time costs and cannot ensure a good coating quality, making them difficult to adapt to the increasingly high production requirements of the aerospace manufacturing industry. Improving the coating process to achieve a controllable coating thickness and uniformity may not only improve the production efficiency and qualification rate but also reduce the weight of structural plates in spacecraft. Screen printing technology has been widely used in the aerospace industry. Hoces [4] used screen printing technology to produce the emitters and metal contacts in solar cells. Erika [5] implemented a local rear-side structure with screen-printed front-side metallization in a solar cell process with dielectric layer passivation. The coating process for structural plates in spacecraft has been improved to rotary screen printing, with the basic principles shown in Figure 1. The rotary screen moves

in the printing direction at a certain rotational speed and printing speed, maintaining a given distance from the structural plate. The adhesive is pressed out from pores in the nickel screen to the substrate under the pressure of the squeegee to coat the adhesive.

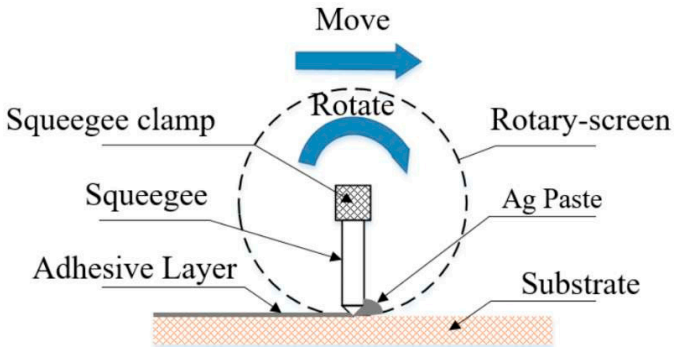

Figure 1. Schematic of rotary screen coating.

Coating quality is affected by many process parameters, such as the adhesive properties, rotary screen mesh, squeegee pressure, rotary screen thickness, and coating speed [6–10]. Combining theory with practice, Dowds [11] provided a detailed introduction to the influencing factors in screen printing, including the adhesive rheology, substrate selection, printing angle, squeegee shape, printing pressure, printing speed, and screen characteristics. Piao [12] analyzed the effects of factors such as the adhesive selection, the mesh size of the screen, sintering temperature, and sintering time on the cathode film in screen printing. Haslehurst and Ekere [13] identified the main factors affecting the deposition height using a factorial experiment and an analysis of variance, including the mesh width, printing direction, squeegee force, and mesh direction. The literature has involved many parameters, as well as complex mathematical models. Therefore, these parameters cannot be coordinated, so it is difficult to guide actual production.

Advanced factories in various countries are gradually transforming and upgrading towards automation, information, and intelligence [14,15]. The production of structural plates for spacecraft should also be equipped with a system for real-time monitoring of important coating parameters so the coating process can be optimized through multi-objective optimization theory, artificial intelligence technology, and the use of production data [16,17]. The Taguchi method is an effective method for reducing the number of tests and optimizing the process parameters, but it is not suitable for multi-objective optimization processes [18–20]. This paper proposes an intelligent technology for optimizing the process parameters in rotary screen coating based on predictive models and multi-objective optimization algorithms. The framework is shown in Figure 2.

Predictive models can establish the relationship between the process parameters and adhesive quality in production data. The models include a Back Propagation Neural Network (BPNN), a Least Squares Support Vector Machine (LSSVM), and Random Forest (RF) [21–24]. Swarm intelligent optimization algorithms have demonstrated potential in optimizing engineering problems [25–28]. The multi-objective grasshopper optimization algorithm (MOGOA) is a new algorithm [29] that has been improved into the CLMOGOA in this paper. It has been proven that the CLMOGOA has better performance than the MOGOA. The Pareto-optimal front solution is used for multi-objective optimization decision-making to meet different indicators in the results [30,31].

In Section 2, the experimental process is designed, and experimental data are collected. In Section 3, three prediction models are introduced and compared to select the optimal model. In Section 4, the original algorithm is improved to enhance its search and convergence capabilities. Section 5 summarizes this paper and looks forward to future development directions.

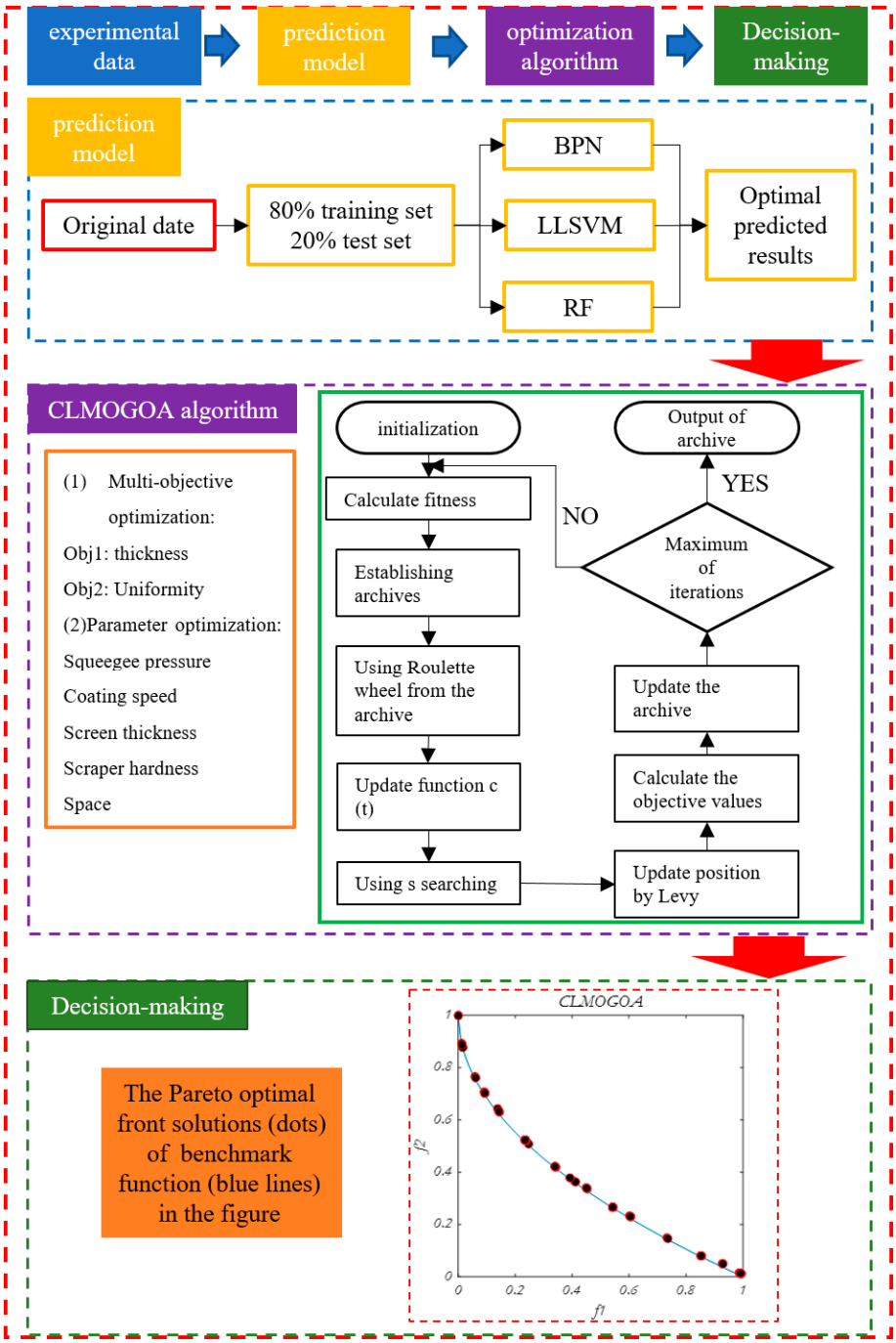

Figure 2. Intelligent technology framework.

2. Design and Evaluation of Experiments

2.1. Experimental Design

The thickness and uniformity of the adhesive layer on the structural plate in spacecraft directly influence the quality of the mounting process. An uneven adhesive layer can result in unstable mounting, while an excessively thick adhesive layer can cause gel overflow during the mounting procedure. In the experiment, five factors were selected for 114 sets of process tests [32]. Each set of parameters was repeatedly used in coating to minimize the experimental errors. Table 1 summarizes these factors and their respective ranges, while Figure 3a illustrates the experimental process.

Table 1. Ranges of process parameters for rotary screen printing.

Printing Factors	Descriptions	Ranges
Screen thickness (μm)	The thickness of the rotary screen	60–120
Squeegee hardness (A)	The hardness of the squeegee	65–85
Squeegee pressure (N)	The pressure on the adhesive by the squeegee	10–50
Space (mm)	The distance between the rotary screen and substrate	0.3–1.6
Coating speed (mm/s)	The moving speed of the rotary screen	10–30

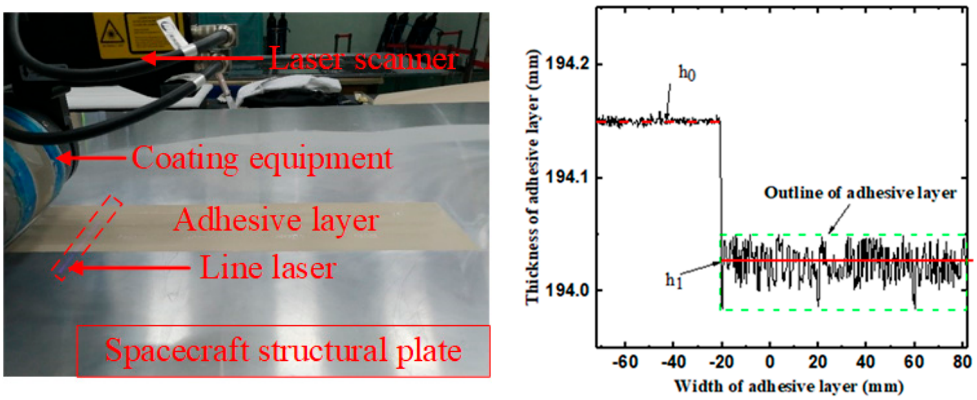

(**a**) (**b**)

Figure 3. Coating test and measurement of adhesive layer thickness. (**a**) Coating test. (**b**) Measurement of adhesive layer thickness. h_0 is the average height between the laser scanner and the structural plate (red dashed line), and h_1 is the average height between the laser scanner and the adhesive layer (red solid line).

2.2. Experimental Evaluation

The purpose of this experiment is to adjust the four factors listed in Table 1 and to conduct coating tests on structural plates in spacecraft. The responses were recorded as the thickness D and roughness R_a of the adhesive, utilizing a VC nano 3D laser scanner (Vision Components, Ettlingen, Germany), as shown in Figure 3b. After recording, a DPS processor (Qt version 5.9.2) was employed to analyze the results obtained from the smart camera. The thickness d of a single laser is defined as follows.

$$d = h_0 - h_1 \tag{1}$$

Roughness is defined as a micro-geometric feature determined by small peaks and valleys with minimal spacing (of less than 1 mm) on the machined surface [33,34]. Consequently, this article employs the concept of roughness in mechanical processing to assess the uniformity of the adhesive layer. The lower the roughness, the more uniform the adhesive layer. The roughness r_a of a single laser is defined as follows:

$$r_a = \frac{\sum_{i=2}^{m} |h_i - h_1|}{m} \tag{2}$$

where h_i is the height of the i-th point, and m is the number of points. The entire adhesive layer thickness D is determined as

$$D = \frac{\sum_{j=1}^{n} d_j}{n} \tag{3}$$

where d_j is the scanning thickness of the j-th laser line. n is the number of laser lines. The roughness R_a of the adhesive layer is defined as

$$R_a = \frac{\sum_{j=1}^{n} r_{aj}}{n} \tag{4}$$

where r_{aj} is the roughness of the j-th laser line. In this study, the main defects of the adhesive layer are lacks, leakage, and intermittency, as shown in the Figure 4.

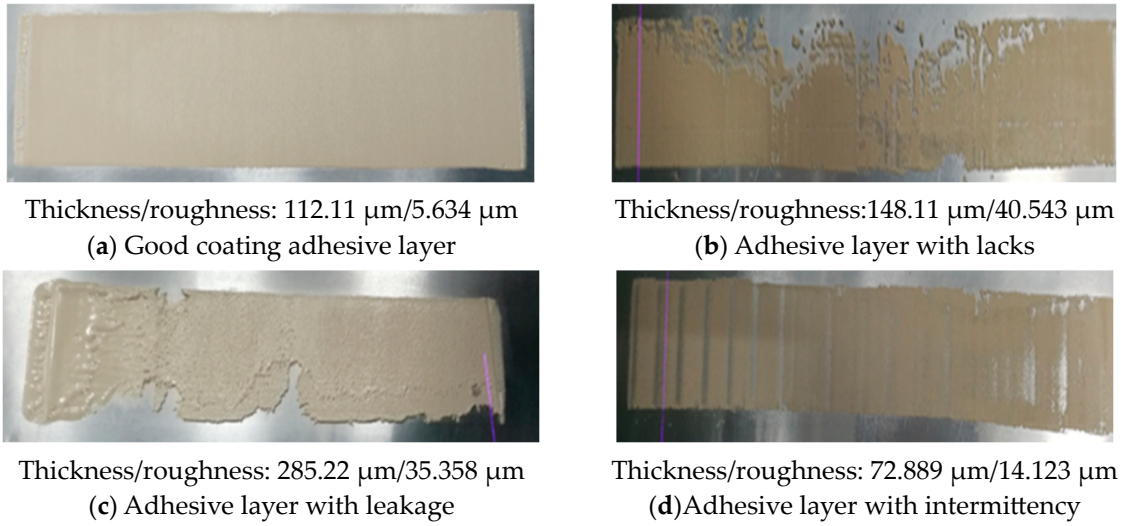

Thickness/roughness: 112.11 μm/5.634 μm
(**a**) Good coating adhesive layer

Thickness/roughness:148.11 μm/40.543 μm
(**b**) Adhesive layer with lacks

Thickness/roughness: 285.22 μm/35.358 μm
(**c**) Adhesive layer with leakage

Thickness/roughness: 72.889 μm/14.123 μm
(**d**)Adhesive layer with intermittency

Figure 4. Comparison of adhesive layer.

3. Forecasting Models

A total of 114 samples were divided into a training set comprising 92 samples and a test set consisting of 22 samples, which were utilized in the prediction models. To mitigate the influence of randomness in the data selection, the model was executed independently 10 times to derive an average performance result. Throughout this process, the training and test sets were randomly selected from the original dataset. The root mean square deviation (RMSE) and the correlation coefficient (R^2) of the three prediction models were subsequently compared.

$$\begin{aligned} \mathrm{RMSE} &= \frac{1}{n}\sqrt{\sum_{i=1}^{n}\left(\frac{X_i - Y_i}{X_i}\right)^2} \\ R^2 &= \frac{\sum_{i=1}^{n}\left(X_i - \overline{X}\right)\left(Y_i - \overline{Y}\right)}{\sqrt{\sum_{i=1}^{n}\left(X_i - \overline{X}\right)^2}\sqrt{\sum_{i=1}^{n}\left(Y_i - \overline{Y}\right)^2}} \end{aligned} \tag{5}$$

where $\overline{X} = \frac{1}{n}\sum_{i=1}^{n} X_i, \overline{Y} = \frac{1}{n}\sum_{i=1}^{n} Y_i$, n is the number of samples, X_i denotes the actual response of sample i, and Y_i is the predicted response of sample i. The lower the RMSE, the lower the prediction error. The correlation coefficient ranges from 0 to 1, with values closer to 1 indicating a stronger correlation of the model. The results satisfy both the RMSE and R^2 requirements, demonstrating that the model effectively captures the relationship between the input and output variables.

3.1. The BPNN Forecasting Model

The Back Propagation Neural Network (BPNN) is a widely utilized machine learning algorithm for establishing predictive models. The critical components include defining the model structure, activation function, loss function, and optimization algorithm, with the objective of enhancing the prediction accuracy through iterative updating of the connection weights and biases. The network architecture consists of an input layer, a hidden layer, and

an output layer. In the current study, five control factors serve as the inputs, while two responses are designated as outputs. The initial number of hidden layer nodes, denoted as n, can be estimated using Equation (6) [17].

$$n = \frac{(Number\ of\ input\ nodes + Number\ of\ output\ nodes)}{2} + \sqrt{Number\ of\ training\ samples} \quad (6)$$

We set the number of training iterations to 1000. The default learning rate is 0.8. After completing multiple training iterations, the prediction results were taken as the average RMSE and R^2, as shown in Table 2.

Table 2. Comparison of different models.

Forecasting Model	BPN		LSSVM		RF	
	Thickness	**Roughness**	**Thickness**	**Roughness**	**Thickness**	**Roughness**
RMSE	1.28	0.2217	1.7851	0.312	0.9151	0.1865
R^2	0.8878	0.8585	0.8543	0.8295	0.9043	0.8878

3.2. The LS-SVM Forecasting Model

The Least Squares Support Vector Machine (LSSVM) is based on a loss function from machine learning [35]. Within its framework, it incorporates two types of norms into the objective function and replaces the in-equality constraints with equality constraints in the SVM. Consequently, the loss function can use a system of linear equations that are derived from the Kuhn–Tucker conditions for solution. For sample x, the prediction model f(x) can be represented by the following equation:

$$f(x) = \sum_{i=1}^{N} \alpha_i K(x, x_i) + b \quad (7)$$

where α_i is the Lagrange multiplier,b is the constant, and N is the number of samples. x_i is the new input sample, and $K(x, x_i)$ is the Gaussian radial basis kernel function (RBF).

$$K(x, x_i) = \exp\left[-||x, x_i||^2 / 2\sigma^2\right] \quad (8)$$

where σ^2 is the kernel parameter. The prediction results were taken as the average RMSE and R^2, as shown in Table 2.

3.3. The RF Forecasting Model

The Random Forest (RF) model is an ensemble learning method with high prediction robustness and accuracy. After inputting a value, the RF model constructs multiple decision trees. For each decision tree, the RF model randomly selects N samples with replacement. The probability of each sample not being selected is $(1 - 1/N)^N$, and when N is large enough, approximately 37% of the samples will not be selected. The samples that have not been selected are called out-of-bag (OOB) data. The OOB data can estimate the error of each decision tree. The average error of K decision trees approximates the generalization error. The prediction results of any decision tree are averaged or weighted-averaged to obtain the final prediction result. When constructing the decision trees, the RF model randomly segments selected features to avoid over-fitting. Given a training sample set S and a sample feature vector dimension M, the primary variable is the number K of decision trees in the model. This paper sets the number of decision trees to 300. The results in terms of the RMSE and R^2 are shown in Table 2.

3.4. Comparison of the Different Models

When comparing the three prediction methods in Table 2, the RF model has the best performance. It has the lowest error and the highest fitting accuracy, so the RF prediction model is used as the fitness function for the optimization algorithm.

4. Multi-Objective Optimization Algorithm

4.1. Multi-Objective Optimization

The problem of multi-objective optimization is described as follows:

$$\begin{gathered} \min F(X) = [f_1(X), f_2(X), \cdots, f_m(X)]^T \\ \text{s.t. } g_j(X) \leq 0, j = 1, 2, \cdots, p \end{gathered} \tag{9}$$

The function $F(X)$ is called the objective function, which evaluates the performance indicators of the design system; $g_j(X)$ is called the constraint function; and X is an n-dimensional design variable. $X = \{\}$ is called the feasible region of the above formula. In practical engineering problems, the goal pursued by decision-makers is to simultaneously optimize various performance indicators. The concept of Pareto optimality is widely applied to multi-objective optimization problems. Below is the definition of Pareto optimality as follows.

Definition 1 (Pareto domination)**.** *Assume two decision vectors, such as* $\vec{x} = (x_1, x_2, \ldots, x_k)$ *and* $\vec{y} = (y_1, y_2, \ldots, y_k)$*. Vector* $\vec{x}$ *is said to dominate vector* $\vec{y}$ *(denote as* $\vec{x} \prec \vec{y}$*), when*

$$\forall i \in \{1, 2, \ldots, k\} : f_i\left(\vec{x}\right) \leq f_i\left(\vec{y}\right) \wedge \exists i \in \{1, 2, \ldots, k\} : f_i\left(\vec{x}\right) < f_i\left(\vec{y}\right) \tag{10}$$

Definition 2 (Pareto-optimal solution)**.** *Assuming* $\vec{x} \in X$ *is a decision vector,* $\vec{x}$ *is said to be a Pareto-optimal solution when*

$$\left\{ \nexists \vec{y} \in X \middle| \vec{y} \prec \vec{x} \right\} \tag{11}$$

Definition 3 (Pareto-optimal set)**.** P_s *is the set of Pareto-optimal solutions:*

$$P_s := \left\{ \vec{x}, \vec{y} \in X \middle| \nexists \vec{y} \prec \vec{x} \right\} \tag{12}$$

Definition 4 (Pareto front)**.** *Pareto front P is a set of Pareto-optimal solutions for all objective functions,*

$$P_f := \left\{ f\left(\vec{x}\right) \middle| \vec{x} \in P_s \right\} \tag{13}$$

4.2. The GOA

The grasshopper optimization algorithm (GOA) simulates the swarming behavior of grasshoppers in nature and has been applied in practical scenarios. The solution is the position of the grasshoppers in the GOA. Therefore, the mathematical formulation for the i-th grasshopper position is given by

$$X_i = S_i + G_i + A_i \tag{14}$$

where S_i simulates social interaction, G_i represents the influence of gravity, and A_i represents the influence of wind. Social interaction plays an important role in the movement of grasshoppers, and the relationship between grasshoppers can be described as follows:

$$s_i = \sum_{\substack{i=1 \\ j \neq i}}^{N} s(d_{ij}) \widehat{d_{ij}} \tag{15}$$

where N is the number of grasshoppers. d_{ij} is the distance between the i-th and j-th grasshopper, calculated as $d_{ij} = |x_j - x_i|$, and $\widehat{d_{ij}} = \frac{x_j - x_i}{d_{ij}}$ is the unit vector of the distance between the i-th and j-th grasshopper. s is a coefficient of social interaction. When s is negative, it indicates mutual exclusion, and when s is positive, it indicates mutual attraction, as defined in Equation (16):

$$s(r) = fe^{\frac{-r}{l}} - e^{-r} \tag{16}$$

where l is an attraction intensity parameter, and f is an attraction scale parameter.

The gravity force G is calculated as follows:

$$G_i = -g\widehat{e_g} \tag{17}$$

where g is the gravitational constant, and $\widehat{e_g}$ indicates a unity vector of g.

The wind advection A in equation (18) is given by

$$A_i = u\widehat{e_w} \tag{18}$$

where u is the wind force constant, and $\widehat{e_w}$ is a unity vector in the direction of wind. Thus, Equation (14) can be rewritten with all components as follows:

$$X_i = \sum_{\substack{i=1 \\ j \neq i}}^{N} s(|x_j - x_i|)\frac{x_j - x_i}{d_{ij}} - g\widehat{e_g} + u\widehat{e_w} \tag{19}$$

When the grasshoppers reach the comfort zone, they still do not exhibit convergence. In order to solve optimization problems and coordinate global and local optimization processes, parameters are introduced to optimize each stage. The improved mathematical model is as follows:

$$X_i = c\left(\sum_{\substack{i=1 \\ j \neq i}}^{N} c\frac{ub_d - lb_d}{2} s(|x_j - x_i|)\frac{x_j - x_i}{d_{ij}}\right) + \widehat{T_d} \tag{20}$$

where ub_d and lb_d are, respectively, the upper and lower bound in the d-th dimension. $\widehat{T_d}$ is the position of the current optimal individual in the d-th dimension. c is the decreasing coefficient of reducing the comfort zone. The parameter c is updated to reduce exploration and increase exploitation in accordance with the number of iterations, as indicated in the following equation:

$$c = c_{max} - t\frac{c_{max} - c_{min}}{T} \tag{21}$$

where $c_{max} = 1$, and $c_{min} = 0.00001$. t indicates the current iteration, and T is the maximum number of iterations.

4.3. The CLMOGOA

The parameter c plays a key role in the integrity of the multi-objective grasshopper optimization algorithm (MOGOA). The parameter c linearly decreases in the initial stage of the algorithm, resulting in an insufficient global exploration ability of the algorithm. With the number of iterations increasing, the descent speed of the algorithm remains unchanged, leading to the premature occurrence of local optimal values, and the rate of convergence is relatively slow. To solve this problem, a curve function $c(t)$ is proposed to replace parameter c to balance the ability for global exploration and local development. This function is defined as follows:

$$c(t) = c_{max} - t^2\frac{c_{max} - c_{min}}{T^2} \tag{22}$$

In Figure 5, the quadratic function c(t) depicted exhibits a decreasing trend over time. During the initial iteration, $c(t)$ changes slowly, facilitating the exploration of a local optimal value that satisfies the specified conditions; after finding the local optimal value, $c(t)$ can quickly converge to the global optimal value to improve the operational efficiency.

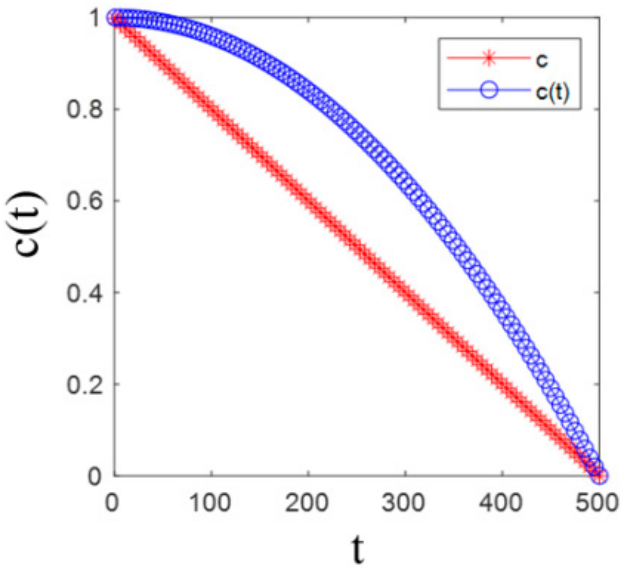

Figure 5. Curves of parameter c and function $c(t)$.

The MOGOA is susceptible to local convergence tendencies and a limited global search capability in nonlinear optimization problems. While the Levy flight strategy improves the algorithm's ability to explore globally, it does not entirely mitigate the risk of local optimization. To enhance the search ability, a novel Levy flight strategy is introduced in this paper, modifying the step factor α from a static to a dynamic value. The revised strategy aims to bolster the algorithm's search effectiveness by adapting the step factor dynamically during the optimization process. The definition is as follows:

$$\alpha(t) = \frac{t}{T_{max}} sinh\left(1 - \frac{t}{T_{max}}\right) * r \tag{23}$$

where r is an adjustable parameter. When r = 3.83, $\alpha(t)$ varies between 0 and 1, and the Levy fight mechanism is enhanced to find the optimal value, as shown in Figure 6.

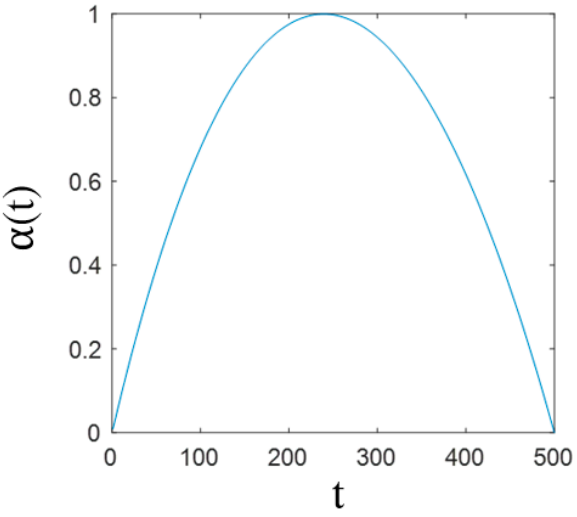

Figure 6. Curve of dynamic step factor.

Following the algorithm update, the Levy flight strategy is used to update the individual position, which achieves the effect of jumping out of the local optimal solution and expanding the search ability. The enhanced Levy fight strategy is incorporated, and the location update method is as follows:

$$x_i^{t+1} = x_i^t + \alpha(t)\frac{\varphi * \mu}{|v|^{\frac{1}{\lambda}}}\left(x_i^t - x_{best}\right) \tag{24}$$

where x_i^t indicates the position of the grasshopper in the current iteration number; x_i^{t+1} indicates the next position of the grasshopper; x_{best} is the current optimal solution; the value of λ is 1.5; and μ and v follow a normal random distribution. The expression for φ is as follows:

$$\varphi = \left| \frac{\gamma(1+\lambda) * sin\left(\pi * \frac{\lambda}{2}\right)}{\gamma\left(\frac{1+\lambda}{2}\right) * \lambda * 2^{\frac{\lambda-1}{2}}} \right|^{\frac{1}{\lambda}} \tag{25}$$

4.4. Analysis of the MOGOA and the CLMOGOA on Test Functions

Zitzler, Deb, and Thiele proposed a test function set for multi-objective optimization problems known as the ZDT function [36]. It contains multiple test functions with different characteristics, such as ZDT1, ZDT2, and ZDT3. In this section, the CLMOGOA was compared with the MOGOA on benchmark test functions to evaluate the overall performance. Inverted generational distance (IGD) was used to assess the convergence performance of the algorithms, which is defined as follows:

$$IGD(P, P^*) = \frac{\sum_{x \in P^*} min_{y \in P} dis(x, y)}{|P^*|} \tag{26}$$

where P^* is a uniformly distributed set of points. P is the point set of the algorithm. $dis(x, y)$ represents the Euclidean metric of points (x, y) in P^* and P. The lower the value of the IGD, the stronger the convergence and the overall performance of algorithms.

We set the maximum number of iterations to 200, the number of populations to 20, and the archive size to 100 in the test sets. Two algorithms were run independently 10 times for statistics. A comparison of the Pareto-optimal front solution on different benchmark functions is shown in Figure 7. The IGD performance of the two algorithms on different benchmark functions is shown in Table 3. It can be observed that the Pareto-optimal front solution of the CLMOGOA has better coverage than that of the MOGOA on all benchmark functions, indicating the effectiveness of the improved algorithm, in Figure 7.

Table 3. Results in terms of the IGD on the test functions employed.

Algorithm		MOGOA	CLMOGOA
ZDT1	Average	0.2030	0.0288
	Median	0.0408	0.0254
	Standard deviation	0.2392	0.0199
ZDT2	Average	0.1718	0.0233
	Median	0.0334	0.0186
	Standard deviation	0.2510	0.0176
ZDT3	Average	0.2687	0.1810
	Median	0.1810	0.0894
	Standard deviation	0.2462	0.2257

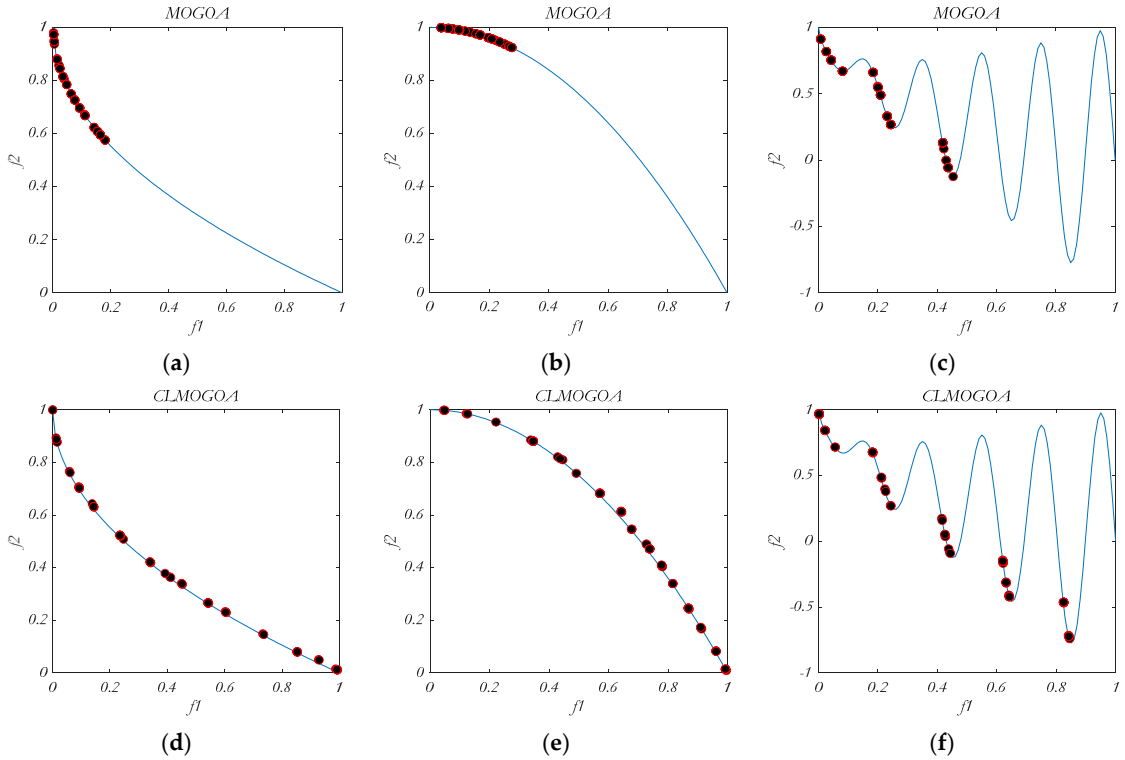

Figure 7. Best Pareto optimal front obtained by the multi objective algorithms on ZDT1, ZDT2, and ZDT3. (**a**) The MOGOA on ZDT1. (**b**) The MOGOA on ZDT2. (**c**) The MOGOA on ZDT3. (**d**) The CLMOGOA on ZDT1. (**e**) The CLMOGOA on ZDT2. (**f**) The CLMOGOA on ZDT3. The dots are the optimal Pareto-optimal fronts. The solid lines are the true Pareto-optimal fronts of the test functions.

It can be seen from Table 3 that compared with that of the MOGOA, the IGD of the CLMOGOA is lower on all three benchmark test functions, so better than that of the MOGOA. Compared to the MOGOA, the CLMGOA has an enhanced ability to find Pareto-optimal front solutions while also having higher convergence and coverage. Therefore, this paper adopts the CLMOGOA to obtain the optimal process parameter combination for rotary screen coating of structural plates in spacecraft.

4.5. The Result of Process Parameter Optimization

The entire optimization process is run in MATLAB 2023b. The RF prediction model is used as the fitness function of the CLMOGOA to obtain the optimal process parameter combination for the rotary screen coating process for structural plates in spacecraft. The thickness of the adhesive layer is required to be between 0.1 and 0.12 mm. The smaller the absolute value of the difference, the more precise the optimization result. The lower the roughness, the more uniform the adhesive layer.

Objective function 1: Minimization of the absolute value of the difference

$$\text{Minimize } f_1 = |RF\_predict([x(1), x(2), x(3), x(4), x(5)]) - 0.11| \tag{27}$$

Objective function 2: Minimization of the roughness

$$\text{Minimize } f_2 = RF\_predict([x(1), x(2), x(3), x(4), x(5)]) \tag{28}$$

The RF prediction model sets the number of decision trees to 300. The CLMOGOA sets the maximum number of iterations to 200, the number of populations to 20, and the archive size to 100. The Pareto optimal front solutions are shown in Figure 8. The optimal combination of process parameters is presented in Table 4.

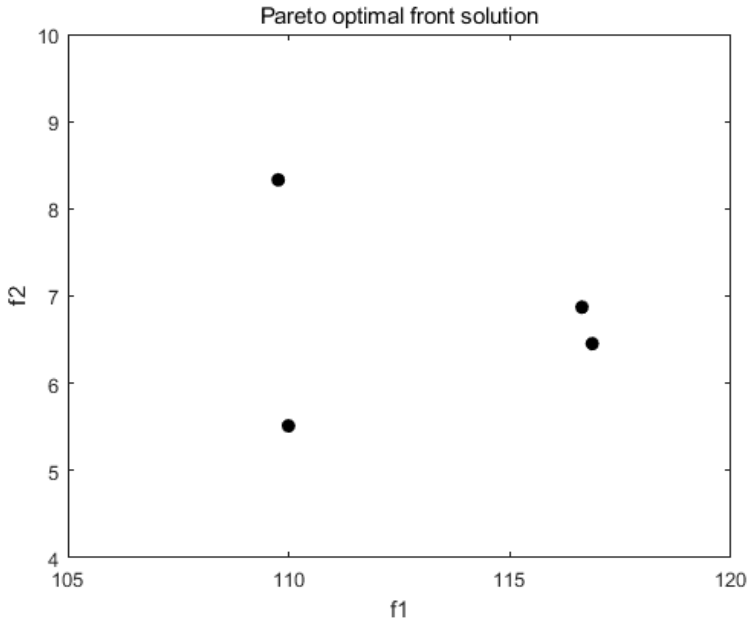

Figure 8. Pareto-optimal front solutions.

Table 4. The archive of the CLMOGOA.

	Control Factors					Forecasting Values	
	Screen Thickness (μm)	**Squeegee Hardness (A)**	**Squeegee Pressure (N)**	**Space (mm)**	**Coating Speed (mm/s)**	**Thickness (μm)**	**Roughness (μm)**
Solution of the archive	118.82	76.61	22.64	0.97	23.95	116.86	6.45
	101.76	74.23	39.45	1.26	16.15	109.99	5.5
	120	75.94	24.05	0.98	25.66	116.6	6.87
	104	74.57	39.89	1.25	15.98	109.76	8.33

In Figure 8, when the screen thickness is 110, the squeegee hardness is 75, the squeegee pressure is 40, the space is 1.26, and the coating speed is 16, the result of the algorithm is optimal. This paper conducted three experiments on all of the parameter combinations in the table, and the coating results were basically consistent with the optimization results. A mounting test was conducted on the coating effect, and there was no overflow or loose installation. After observing the actual production for four days, the coating effect met the production requirements, improved the coating efficiency, and reduced the cost of mounting.

5. Conclusions

An intelligent technology based on predictive models and optimization algorithms is proposed to solve the issue of there being numerous process parameters in rotary screen coating. According to numerous works in the literature and parameter characteristics, five important process parameters were selected as the control factors, and the thickness and uniformity of the adhesive layer were selected as the response factors. In training BPN, LSSVM, and RF prediction models with experimental data, the RF's prediction results are the most accurate. Finally, the MOGOA was improved into the CLMOGOA from the aspects of convergence speed, search range, and local optimization. It was demonstrated that the CLMOGOA has better performance than that of the MOGOA. After obtaining multiple sets of optimal process parameters by combining the RF prediction model and the CLMOGOA, coating experiments were conducted on structural plates for spacecraft. The efficiency and quality of coating were improved, which is of great significance for the coating process for structural plates in aerospace. Compared to manual coating, this

intelligent technology reduces the number of experiments required. However, in order to obtain precise results, many experiments were still conducted. In future work, it will be necessary to obtain more accurate results using a smaller sample size.

Author Contributions: Methodology, P.L.; investigation, Y.C.; data curation, Y.C.; writing—original draft, Y.G.; writing—review and editing, P.L. and Y.S.; supervision, P.L. and Y.S.; funding acquisition, X.C. All authors have read and agreed to the published version of the manuscript.

Funding: This work was supported by the National Key R&D Program of China (Grant No. 2017YFB0309800) and Fundamental Research Funds for the Central Universities (Grant No.21D110326).

Data Availability Statement: The raw data supporting the conclusions of this article will be made available by the authors on request.

Conflicts of Interest: The authors declare no conflicts of interest.

References

1. Curtis, S.A.; Rilee, M.L.; Clark, P.E.; Marr, G.C. Use of swarm intelligence in spacecraft constellations for the resource exploration of the asteroid belt. In Proceedings of the Third International Workshop on Satellite Constellations and Formation Flying, Pisa, Italy, 24–26 February 2003.
2. Galbraith, J. United States creates the US space command and the US space force to strengthen military capabilities in space. *Am. J. Int. Law* **2020**, *114*, 323–326.
3. Jianfa, H.U.; Chunli, X. Comment on the building blocks for the development of international framework on space resource activities (draft). *J. Beijing Univ. Aeronaut. Astronaut. Soc. Sci. Ed.* **2019**, *32*, 136–141.
4. Hoces, I.; Azkona, N.; Freire, I.; Pérez, L.; Lago, R.; Recart, F.; Jimeno, J.C.; Kerp, H.; Albertsen, K.; Shaikh, A. *An Industrial Process for Bifacial Solar Cells Based on Screen-Printing Techniques*; Contract No. TREN/04/FP6EN/S07.34325/503105; ResearchGate: 2022.
5. Pavlović, R.; Dastgheib-Shirazi, A.; Book, F.; Raabe, B.; Hahn, G. Large area solar cells with screen printed front side metallization and dielectric rear side passivation. In Proceedings of the 4th European Photovoltaic Solar Energy Conference, Munich, Germany, 21–25 September 2009.
6. Drabczyk, K.; Panek, P. Influence of screen printing parameters on the front metallic electrodes geometry of solar cells. *Circuit World* **2014**, *40*, 23–26. [CrossRef]
7. Kuo, H.-P.; Yang, C.-F.; Huang, A.-N.; Wu, C.-T.; Pan, W.-C. Preparation of the working electrode of dye-sensitized solar cells: Effects of screen printing parameters. *J. Taiwan Inst. Chem. Eng.* **2014**, *45*, 2340–2345. [CrossRef]
8. Ichinose, K. Rotary Screen Textile Printing Machine. EP0863000A1, 9 September 1998.
9. Hawkyard, C.J.; Miah, A.S. The parameters of rotary screen printing. *J. Soc. Dye. Colour* **1987**, *103*, 27–31. [CrossRef]
10. Rodriguez, G.; Baldwin, D.F. Analysis of solder paste release in fine pitch stencil printing processes. *J. Electron. Packag.* **1999**, *121*, 169–178. [CrossRef]
11. Dowds, B.F. Variables in Textile Screen Printing. *J. Soc. Dye. Colour* **1970**, *86*, 512–519. [CrossRef]
12. Piao, J.; Sun, K.; Zhang, N.; Xu, S. A study of process parameters of LSM and LSM–YSZ composite cathode films prepared by screen-printing. *J. Power Sources* **2008**, *175*, 288–295. [CrossRef]
13. Haslehurst, L.; Ekere, N.N. Parameter Interactions in Stencil Printing of Solder Paste. *J. Electron Manuf.* **2012**, *6*, 307–316. [CrossRef]
14. Scanzio, S.; Wisniewski, L.; Gaj, P. Heterogeneous and dependable network in industry—A survey. *Comput. Ind.* **2021**, *125*, 103388. [CrossRef]
15. Ponalagusamy, R.; Kannan, E.; Michael, A. A Huffman Decoding Algorithm in Mobile Robot Platform. *Inf. Technol. J.* **2007**, *6*, 310–316.
16. Tian, H.; Tian, C.; Yuan, C.; Li, K. Dynamic operation optimization based on improved dynamic multi-objective dragonfly algorithm in continuous annealing process. *J. Ind. Manag. Optim.* **2023**, *19*, 6159–6181. [CrossRef]
17. Wang, Y.; Liu, Y.; Sun, Y. A hybrid intelligence technique based on the Taguchi method for multi-objective process parameter optimization of the 3D additive screen printing of athletic shoes. *Sage J.* **2019**, *90*, 1067–1083. [CrossRef]
18. Omprakasam, S.; Marimuthu, K.; Raghu, R.; Velmurugan, T. Statistical Modelling and Optimization of TIG Welding Process Parameters Using Taguchi's Method. *J. Mech. Eng.* **2022**, *68*, 200–209.
19. Uray, E.; Carbas, S.; Geem, Z.W.; Kim, S. Parameters Optimization of Taguchi Method Integrated Hybrid Harmony Search Algorithm for Engineering Design Problems. *Mathematics* **2022**, *10*, 327. [CrossRef]
20. Raveendran, P.; Alagarsamy, S.V.; Ravichandran, M.; Meignanamoorthy, M. Effect of machining parameters on surface roughness for aluminium matrix composite by using Taguchi method with decision tree algorithm. *Surf. Rev. Lett.* **2021**, *28*, 2150021. [CrossRef]
21. He, S.; Xie, M.; Tontiwachwuthikul, P.; Chan, C.; Li, J. Self-adapting anti-surge intelligence control and numerical simulation of centrifugal compressors based on RBF neural network. *Energy Rep.* **2022**, *8*, 2434–2447. [CrossRef]

22. Huang, Y.; Zhang, J.; Tze Ann, F.; Ma, G. Intelligent mixture design of steel fibre reinforced concrete using a support vector regression and firefly algorithm based multi-objective optimization model. *Constr. Build. Mater.* **2020**, *260*, 120457. [CrossRef]
23. Zhao, J.; Yang, D.; Wu, J.; Meng, X.; Li, X.; Wu, G.; Miao, Z.; Chu, R.; Yu, S. Prediction of temperature and CO concentration fields based on BPNN in low-temperature coal oxidation. *Thermochim. Acta* **2021**, *695*, 178820. [CrossRef]
24. Liang, J.-X.; Zhao, J.-F.; Sun, N.; Shi, B.-J. Random Forest Feature Selection and Back Propagation Neural Network to Detect Fire Using Video. *J. Sens.* **2022**, *2022*, 5160050. [CrossRef]
25. Gong, M.; Cai, Q.; Chen, X.; Ma, L. Complex Network Clustering by Multi-objective Discrete Particle Swarm Optimization Based on Decomposition. *IEEE Trans. Evol. Comput.* **2014**, *18*, 82–97. [CrossRef]
26. Marjalili, S.; Mirjalili, S.M.; Lewis, A. Grey Wolf Optimizer. *Adv. Eng. Soft.* **2014**, *69*, 46–61. [CrossRef]
27. Josef, T. Differential Evolution: Competitive Setting of Control Parameters. In Proceedings of the International Multiconference on Computer Science and Information Technology, Washington, DC, USA, 1–3 August 2006; pp. 207–213.
28. Mirjalili, S.; Jangir, P.; Saremi, S. Multi-objective ant lion optimizer: A multi-objective optimization algorithm for solving engineering problems. *Appl. Intell.* **2017**, *46*, 79–95. [CrossRef]
29. Mirjalili, S.Z.; Mirjalili, S.; Saremi, S.; Faris, H. Grasshopper optimization algorithm for multi-objective optimization problems. *Appl. Intell.* **2018**, *48*, 805–820. [CrossRef]
30. Ngatchou, P.; Zarei, A.; Elsharkawi, M.A. Pareto Multi Objective Optimization. In Proceedings of the International Conference on Intelligent Systems Application to Power Systems, Arlington, VA, USA, 6–10 November 2005; IEEE: Piscataway, NJ, USA, 2005.
31. Ghahraloud, H.; Farsi, M. Modeling, operability analysis and optimization of isooctane production over solid catalyst. *Pet. Sci. Technol.* **2019**, *37*, 997–1007. [CrossRef]
32. Pan, J.; Tonkay, G.L.; Quintero, A. Screen printing process design of experiments for fine line printing of thick film ceramic substrates. In Proceedings of the International Symposium on Microelectronics, San Diego, CA, USA, 1 November 1998; Volume 9, pp. 203–213.
33. Bintara, R.D.; Pradana, Y.R.A.; Aminnudin, A.; Suryanto, H. The orientation and high-quality effect of deposit layer to surface roughness on fdm 3d printed part. *Key Eng. Mater.* **2023**, *940*, 95–99. [CrossRef]
34. Abd Alsamieh, M. Ultrathin film formation under combined effect of surface roughness and surface force for elastohydrodynamic lubrication of point contact problems. *Ind. Lubr. Tribol.* **2022**, *74*, 597–608. [CrossRef]
35. Suykens, J.A.K.; Vandewalle, J. Least Squares Support Vector Machine Classifiers. *Neural Process. Lett.* **1999**, *9*, 293–300. [CrossRef]
36. Zitzler, E.; Deb, K.; Thiele, L. Comparison of Multiobjective Evolutionary Algorithms: Empirical Results. *Evol. Comput.* **2000**, *8*, 173–195. [CrossRef]